Applications of Mathematics

Vít Dolejší; Filip Roskovec

Goal-oriented error estimates including algebraic errors in discontinuous Galerkin discretizations of linear boundary value problems

Applications of Mathematics, Vol. 62 (2017), No. 6, 579–605

Persistent URL: http://dml.cz/dmlcz/146999

62 (2017) APPLICATIONS OF MATHEMATICS No. 6, 579–605

GOAL-ORIENTED ERROR ESTIMATES INCLUDING ALGEBRAIC ERRORS IN DISCONTINUOUS GALERKIN DISCRETIZATIONS OF LINEAR BOUNDARY VALUE PROBLEMS

Vít Dolejší, Filip Roskovec, Praha

Received June 28, 2017. First published December 12, 2017.

Dedicated to Professor Miloslav Feistauer on the occasion of his 75th birthday.

Abstract. We deal with a posteriori error control of discontinuous Galerkin approximations for linear boundary value problems. The computational error is estimated in the framework of the Dual Weighted Residual method (DWR) for goal-oriented error estimation which requires to solve an additional (adjoint) problem. We focus on the control of the algebraic errors arising from iterative solutions of algebraic systems corresponding to both the primal and adjoint problems. Moreover, we present two different reconstruction techniques allowing an efficient evaluation of the error estimators. Finally, we propose a complex algorithm which controls discretization and algebraic errors and drives the adaptation of the mesh in the close to optimal manner with respect to the given quantity of interest.

Keywords: quantity of interest; discontinuous Galerkin; a posteriori error estimate; algebraic error

MSC 2010: 65N15, 65N30, 65N50

1. Introduction

The goal-oriented error estimates exhibit a perspective and efficient tool for numerical simulations of many engineering problems since they are able to give information about the error of a *quantity of interest* which is more relevant in practical applications than error estimates derived in energy norms. The quantity of interest is usually represented by a (linear) functional $J(u)$, where u is the exact solution of the

The research of V. Dolejší was supported by Grant No. 17-01747S of the Czech Science Foundation. The research of F. Roskovec was supported by the Charles University, project GA UK No. 92315.

DOI: 10.21136/AM.2017.0173-17

given problem. We refer to [4], [6], [13], where the *dual weighted residual* (DWR) estimates dealing with this subject were introduced. This approach requires, in addition to the solution of the original (primal) problem, also to solve the dual (or adjoint) problem. The discretization of the primal and dual problems leads to two linear algebraic systems, which are usually solved by a suitable iterative technique. Therefore, the error of the resulting solution and its error estimate are influenced by the error resulting from inexact solution of both algebraic systems.

In this paper we deal with *discontinuous Galerkin* discretization of a linear convection-reaction-diffusion equation and the corresponding a posteriori error estimates of $J(u) - J(u_h)$, where u_h is the approximate solution. Following the ideas from [2], we take into account also the *algebraic error* resulting from inaccurate solution of the algebraic systems mentioned above. This aspect was considered in [21] with the emphasis on the multigrid methods for conforming finite element methods. The novelty of our approach is the consideration of the algebraic error of the dual problem, which was not taken into account in [21]. Then we are able to balance the discretization and algebraic errors for the primal as well as for the dual problem.

The goal oriented error estimates require a sufficiently accurate approximation of the solution of the (continuous) dual problem. One possibility is to solve the dual problem on globally refined mesh, which is time-consuming. In this paper, we present two different reconstruction techniques allowing an efficient and accurate approximation of the solution of the dual problem. This way of post-processing is commonly used for finite element computations, see e.g. [24], but in DG discretizations most of the methods for goal-oriented error estimation described in literature, e.g. [18], [16], are based on globally higher-order solution of the dual problem.

Further, we propose an adaptive algorithm including stopping criteria for the iterative solutions of the primal and dual algebraic problems.

Finally, two kinds of numerical experiments are presented. We compare the performance of the local reconstructions to the globally higher order dual solution, and the decrease of the algebraic errors, when employing the algebraic estimators, is demonstrated.

The outline of the paper is as follows: in Section 2, we start with the discontinuous Galerkin (DG) discretization of the linear convection-diffusion-reaction problem and we derive the goal-oriented error estimates based on the primal and dual residual, respectively. Special attention is paid to the adjoint consistency of the discretization of the dual problem. In Section 3, we present two possibilities of the approximation of the unknown dual solution z on triangular meshes with varying polynomial approximation degree. Further, the error estimates of the quantity of interest including the algebraic errors is derived in Section 4. Numerical experiments documenting the performance of this approach are presented in Section 5.

2. Problem description

In the following, we use the standard notation for the Lebesgue spaces—$L^p(\Omega)$, Sobolev spaces—$W^{k,p}(\Omega)$, $H^k(\Omega) = W^{k,2}(\Omega)$ and the space of polynomial functions up to the degree k defined on a domain $M \subset \mathbb{R}^d$ is denoted $P^k(M)$.

Let $\Omega \subset \mathbb{R}^d$ be a bounded polygonal domain with Lipschitz boundary. Moreover, let the vector valued function $\boldsymbol{b} = \{b_i\}_{i=1}^d$ be a linear convection coefficient whose entries b_i are Lipschitz continuous real-valued functions in Ω, c denotes the reaction coefficient, and $\mathbb{A} = \{a_{i,j}\}_{i,j=1}^d$ is a symmetric diffusion tensor with bounded piecewise continuous real-valued entries, satisfying the elliptic property $\boldsymbol{\zeta}^{\mathrm{T}}\mathbb{A}(x)\boldsymbol{\zeta} \geqslant 0$ for all $\boldsymbol{\zeta} \in \mathbb{R}^d$, a.e. $x \in \Omega$.

By $\boldsymbol{n}(x)$ we denote the unit outward normal vector to $\partial\Omega$ at $x \in \partial\Omega$. We define a disjoint decomposition of the boundary $\partial\Omega$ by

$$\begin{aligned}
\Gamma_0 &:= \{x \in \partial\Omega\colon\ \boldsymbol{n}(x)^{\mathrm{T}}\mathbb{A}(x)\boldsymbol{n}(x) > 0\},\\
\Gamma_- &:= \{x \in \partial\Omega \setminus \Gamma_0\colon\ \boldsymbol{b}(x)\cdot\boldsymbol{n}(x) < 0\},\\
\Gamma_+ &:= \{x \in \partial\Omega \setminus \Gamma_0\colon\ \boldsymbol{b}(x)\cdot\boldsymbol{n}(x) \geqslant 0\}.
\end{aligned}$$

Obviously, these sets are disjoint and $\partial\Omega = \Gamma_0 \cup \Gamma_- \cup \Gamma_+$. Further, we divide Γ_0 into two disjoint subsets Γ_D and Γ_N, see Figure 1. We assume that $\Gamma_- \cup \Gamma_D \neq \emptyset$ and that $\boldsymbol{b}\cdot\boldsymbol{n} \geqslant 0$ on Γ_N whenever $\Gamma_N \neq \emptyset$.

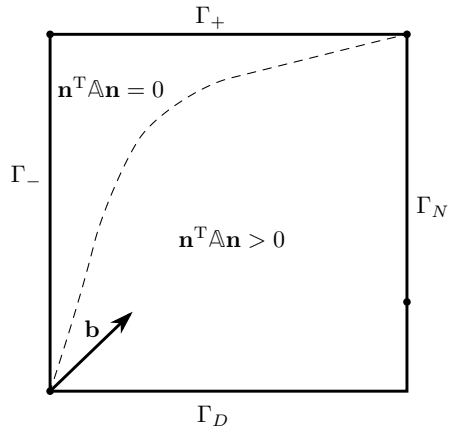

Figure 1. Example of the division of the boundary $\partial\Omega$ into Γ_-, Γ_+, and $\Gamma_0 = \Gamma_D \cup \Gamma_N$.

We consider the linear convection-diffusion-reaction model problem

$$\mathcal{L}u := -\nabla\cdot\mathbb{A}\nabla u + \nabla\cdot(\boldsymbol{b}u) + cu = f \quad \text{in } \Omega, \tag{2.1a}$$

$$u = u_D \quad \text{on } \Gamma_D \cup \Gamma_-, \tag{2.1b}$$

$$\mathbb{A}\nabla u\cdot\boldsymbol{n} = g_N \quad \text{on } \Gamma_N, \tag{2.1c}$$

where $u\colon \Omega \to \mathbb{R}$ is an unknown scalar function. Since the diffusion may degenerate in some parts of Ω, problem (2.1) has to be considered as a first-order PDE in those parts and hence no boundary condition can be set on Γ_+. This kind of problems is termed "partial differential equations with nonnegative characteristic form" in [19].

We assume that the data satisfy $f \in L^2(\Omega)$, u_D is the trace of some $u^* \in H^1(\Omega)$ on $\Gamma_D \cup \Gamma_-$, $g_N \in L^2(\Gamma_N)$, $c \in L^\infty(\Omega)$. Further, we assume that there exists $c_0 > 0$ such that $c(x) + \frac{1}{2}\nabla \cdot \boldsymbol{b}(x) \geqslant c_0$ a.e. $x \in \Omega$. Let us note that this assumption is not restrictive, see e.g. [9], Section 4.6.1.

We proceed to the weak formulation of (2.1).

Definition 2.1. A function $u \in H^1(\Omega)$ is called the *weak solution* of (2.1) if $u - u^* \in H^1_D(\Omega) := \{v \in H^1(\Omega);\ v\big|_{\Gamma_D \cup \Gamma_-} = 0\}$ and

$$a(u, \varphi) = l(\varphi) \quad \forall\, \varphi \in H^1_D(\Omega), \tag{2.2}$$

where

$$a(u,\varphi) := \int_\Omega \mathbb{A}\nabla u \cdot \nabla\varphi \,\mathrm{d}x - \int_\Omega (u\boldsymbol{b} \cdot \nabla\varphi - cu\varphi)\,\mathrm{d}x + \int_{\Gamma_+ \cup \Gamma_N} \boldsymbol{b} \cdot \boldsymbol{n} u\varphi \,\mathrm{d}S,$$
$$l(\varphi) := \int_\Omega f\varphi \,\mathrm{d}x + \int_{\Gamma_N} g_N \varphi \,\mathrm{d}S, \quad u, \varphi \in H^1(\Omega).$$

The well-posedness of the boundary value problem (2.2), in the case of homogeneous boundary conditions, is shown in [20].

2.1. DG discretization of the problem. For the DG discretization we introduce a partition $\mathcal{T}_h$ covering $\overline{\Omega}$ consisting of finite number of closed d-dimensional simplices K with mutually disjoint interiors. The boundary of the element $K \in \mathcal{T}_h$ will be denoted by ∂K, its diameter by $h_K = \operatorname{diam}(K)$ and $|K|$ will be its d-dimensional Lebesgue measure.

By $\mathscr{F}_h$ we denote the union of all faces contained in the partition $\mathcal{T}_h$ and by $\mathscr{F}_h^I$, $\mathscr{F}_h^D$ the union of the interior and Dirichlet boundary faces, respectively. Further, let $\mathscr{F}_h^{ID} := \mathscr{F}_h^I \cup \mathscr{F}_h^D$. For each face $\Gamma \subset \mathscr{F}_h^I$ there exist two neighbouring elements K_L, $K_R \in \mathcal{T}_h$ such that $\Gamma = K_L \cap K_R$. It is possible to define a unit normal vector $\boldsymbol{n} = (n_1, \ldots, n_d)$ at almost every point of $\mathscr{F}_h$. The orientation of $\boldsymbol{n}$ can be chosen arbitrarily for the interior faces, so we can assume that $\boldsymbol{n} = \boldsymbol{n}_{K_L} = -\boldsymbol{n}_{K_R}$. Further, for $K \in \mathcal{T}_h$ we set $\partial K^- := \{x \in \partial K;\ \boldsymbol{b} \cdot \boldsymbol{n}(x) < 0\}$ and similarly $\partial K^+ := \{x \in \partial K;\ \boldsymbol{b} \cdot \boldsymbol{n}(x) \geqslant 0\}$.

We assume that there exists $h_0 > 0$ such that $\{\mathcal{T}_h\}_{h \in (0, h_0)}$ is a system of triangulations which is *shape-regular* and *locally quasi-uniform*, see e.g. [9]. We do not require the conforming properties known from finite element methods. Therefore,

the triangulations $\mathcal{T}_h$ could contain the so called *hanging nodes*. Over the triangulation $\mathcal{T}_h$ we define the so-called *broken Sobolev space* over the triangulation $\mathcal{T}_h$ as $H^s(\Omega, \mathcal{T}_h) = \{v \in L^2(\Omega),\ v\big|_K \in H^s(K) \text{ for all } K \in \mathcal{T}_h\}$ with the norm and the semi-norm $\|v\|_{H^s(\Omega,\mathcal{T}_h)} = \Big(\sum\limits_{K\in\mathcal{T}_h} \|v\|^2_{H^s(K)}\Big)^{1/2}$ and $|v|_{H^s(\Omega,\mathcal{T}_h)} = \Big(\sum\limits_{K\in\mathcal{T}_h} |v|^2_{H^s(K)}\Big)^{1/2}$, respectively.

Discontinuous Galerkin method is very convenient for *hp*-adaptation. Therefore, to each $K \in \mathcal{T}_h$ we assign its local polynomial degree p_K. Then we define the set $\mathtt{p} := \{p_K;\ K \in \mathcal{T}_h\}$ and the finite dimensional space

$$S_h^{\mathtt{p}} = \{v \in L^2(\Omega);\ v\big|_K \in P^{p_K}(K)\ \forall\, K \in \mathcal{T}_h\}. \tag{2.3}$$

The dimension of $S_h^{\mathtt{p}}$ corresponding to the number of degrees of freedom $N_h^{\mathtt{p}}$ can be calculated as $N_h^{\mathtt{p}} := \dim S_h^{\mathtt{p}} = \sum\limits_{K\in\mathcal{T}_h} \binom{p_k+d}{d}$.

Let $\Gamma \subset \mathscr{F}_h^I$, $v \in H^1(\Omega, \mathcal{T}_h)$. We introduce the notation $v_L = \text{trace of } v\big|_{K_L}$ on Γ, and $v_R = \text{trace of } v\big|_{K_R}$ on Γ, Further, we denote the jump of v on Γ by $[\![v]\!] = v_L - v_R$ and its mean value by $\langle v\rangle = \frac{1}{2}(v_L + v_R)$. On $\Gamma \subset \mathscr{F}_h^D$ we set $[\![v]\!] = \langle v\rangle = v_L$, where K_L is such an element that $\Gamma = K_L \cap \partial\Omega$. Given an element $K \in \mathcal{T}_h$ we denote by v^- the exterior trace of v defined on $\partial K \setminus \partial\Omega$, the interior trace on ∂K will be denoted simply by v.

We discretize the equation (2.2) using the interior penalty Galerkin method (IPG), see e.g. [9], Section 4.6 or [19]. For $u, \varphi \in H^2(\Omega, \mathcal{T}_h)$ we define the forms

$$\begin{aligned}
A_h(u,\varphi) :=\ & \sum_{K\in\mathcal{T}_h} \int_K \mathbb{A}\nabla u \cdot \nabla\varphi \,\mathrm{d}x \\
& - \sum_{\Gamma\in\mathscr{F}_h^{ID}} \int_\Gamma \langle \mathbb{A}\nabla u\rangle \cdot \boldsymbol{n}[\![\varphi]\!] + \theta\langle \mathbb{A}\nabla\varphi\rangle \cdot \boldsymbol{n}[\![u]\!] \,\mathrm{d}S,
\end{aligned} \tag{2.4a}$$

$$J_h^\sigma(u,\varphi) := \sum_{\Gamma\in\mathscr{F}_h^{ID}} \int_\Gamma \sigma[\![u]\!][\![\varphi]\!] \,\mathrm{d}S, \tag{2.4b}$$

$$\begin{aligned}
B_h(u,\varphi) :=\ & \sum_{K\in\mathcal{T}_h} \Big(-\int_K u\boldsymbol{b}\cdot\nabla\varphi - cu\varphi \,\mathrm{d}x \\
& + \int_{\partial K^+} \boldsymbol{b}\cdot\boldsymbol{n}_K u\varphi \,\mathrm{d}S + \int_{\partial K^-\setminus\partial\Omega} \boldsymbol{b}\cdot\boldsymbol{n}_K u^-\varphi \,\mathrm{d}S \Big),
\end{aligned} \tag{2.4c}$$

$$\begin{aligned}
l_h(\varphi) :=\ & \int_\Omega f\varphi x \,\mathrm{d}x + \int_{\Gamma_N} g_N\varphi \,\mathrm{d}S - \sum_{K\in\mathcal{T}_h} \int_{\partial K^-\cap\partial\Omega} (\boldsymbol{b}\cdot\boldsymbol{n}) u_D\varphi \,\mathrm{d}S \\
& + \sum_{\Gamma\in\mathscr{F}_h^D} \int_\Gamma (\sigma\varphi - \theta\mathbb{A}\nabla\varphi\cdot\boldsymbol{n}) u_D \,\mathrm{d}S.
\end{aligned} \tag{2.4d}$$

The choice of $\theta \in \{-1, 0, 1\}$ leads to the nonsymmetric (NIPG), incomplete (IIPG), and symmetric (SIPG) variant of the discontinuous Galerkin method. The penalty parameter σ is chosen by $\sigma\big|_\Gamma = \sigma_\Gamma = \varepsilon C_W h_\Gamma^{-1}$, $\Gamma \in \mathscr{F}_h^{ID}$, where ε denotes the amount of diffusivity ($\approx |\mathbb{A}|$), $h_\Gamma = \operatorname{diam}\Gamma$ and $C_W > 0$ has to be chosen large enough to guarantee convergence of the method, see [9]. Further, we introduce the DG-norm

$$\begin{aligned}(2.5)\quad \|\!|v|\!\|_{\mathrm{DG}} := \sum_{K\in\mathcal{T}_h} \big(&\|\mathbb{A}^{1/2}\nabla v\|_K^2 + \tfrac{1}{2}\|v\|_{\partial K^-\cap(\Gamma_D\cup\Gamma_-)}^2 + \tfrac{1}{2}\|\!|[\![v]\!]|\!\|_{\partial K^-\setminus\partial\Omega}^2 \\ &+ \tfrac{1}{2}\|v\|_{\partial K^+\cap\partial\Omega}^2 + \|c_0 v\|_K^2\big) + \int_{\Gamma\in\mathscr{F}_h^{ID}} (\sigma[\![v]\!]^2 + \sigma^{-1}\langle\mathbb{A}\nabla v\cdot\boldsymbol{n}\rangle^2)\,\mathrm{d}S,\end{aligned}$$

where $\|\cdot\|_M$ denotes the standard L^2-norm over the domain M. We use the convention that the edges Γ, where $\boldsymbol{n}^{\mathrm{T}}\mathbb{A}\boldsymbol{n} = 0$ are omitted from the integration in the form $J_h^\sigma(\cdot,\cdot)$ and in the DG-norm.

Finally, we put

$$(2.6)\qquad a_h(u,\varphi) := A_h(u,\varphi) + J_h^\sigma(u,\varphi) + B_h(u,\varphi), \quad u,\varphi \in H^2(\Omega,\mathcal{T}_h).$$

We are ready to define the discrete problem.

Definition 2.2. We say that $u_h \in S_h^{\mathfrak{p}}$ is the *approximate solution* of (2.2) if

$$(2.7)\qquad a_h(u_h,\varphi_h) = l_h(\varphi_h) \quad \forall\,\varphi_h \in S_h^{\mathfrak{p}}.$$

Lemma 2.1. *The discrete problem* (2.7) *is consistent with the weak formulation* (2.2)*, i.e., the exact solution* $u \in H^2(\Omega)$ *satisfies*

$$(2.8)\qquad a_h(u,\varphi) = l_h(\varphi) \quad \forall\,\varphi \in H^2(\Omega,\mathcal{T}_h).$$

P r o o f. See e.g. [9], Chapters 2 and 3, [16]. □

This gives us the Galerkin orthogonality of the exact and the discrete solutions

$$(2.9)\qquad a_h(u-u_h,\varphi_h) = 0 \quad \forall\,\varphi_h \in S_h^{\mathfrak{p}},$$

which is a crucial property (not only) in goal-oriented estimates.

2.2. Quantity of interest. The goal of the whole computation process is to determine the value of the *quantity of interest* $J(u)$, where J is a linear functional defined for the weak as well as the approximate solutions. It was shown in [17]

that the primal problem (2.1), the corresponding dual problem and the target functional $J(u)$ have to satisfy the so-called *compatibility condition* which together with the *consistency* of the numerical method and the *adjoint consistency* guarantee the regularity of the dual solution and then the optimal order of convergence. The low regularity of the solution of the dual problem causes a suboptimal convergence rate of the DWR error estimate, see [17], [15].

We consider the functional J in the form

$$J(u) = \int_\Omega j_\Omega(x)u(x)\,\mathrm{d}x + \int_{\Gamma_D} j_{\Gamma_D}\mathbb{A}\nabla u\cdot\boldsymbol{n}\,\mathrm{d}S + \int_{\Gamma_+\cup\Gamma_N} j_{\Gamma_N}u\,\mathrm{d}S, \tag{2.10}$$

where $j_{\Gamma_D}, j_{\Gamma_N} \in L^2(\partial\Omega)$ and $j_\Omega \in L^2(\Omega)$ are given functions, typically characteristic functions of some subdomains in $\partial\Omega$ or Ω, respectively.

The adjoint operator to $\mathcal{L}$ is defined by $\mathcal{L}^*v = -\nabla\cdot\mathbb{A}\nabla v - \boldsymbol{b}\cdot\nabla v + cv$ and the dual problem corresponding to the target functional (2.10) reads in its strong formulation: Find a function $z\colon\ \Omega\to\mathbb{R}$ such that

$$-\nabla\cdot\mathbb{A}\nabla z - \boldsymbol{b}\cdot\nabla z + cz = j_\Omega \quad \text{in } \Omega, \tag{2.11a}$$

$$z = -j_{\Gamma_D} \quad \text{on } \Gamma_D, \tag{2.11b}$$

$$\mathbb{A}\nabla z\cdot\boldsymbol{n} + \boldsymbol{b}\cdot\boldsymbol{n}z = j_{\Gamma_N} \quad \text{on } \Gamma_N, \tag{2.11c}$$

$$\boldsymbol{b}\cdot\boldsymbol{n}z = j_{\Gamma_N} \quad \text{on } \Gamma_+. \tag{2.11d}$$

The dual problem (2.11) contains a Newton boundary condition on Γ_N, but since $\boldsymbol{b}\cdot\boldsymbol{n} \geqslant 0$ on Γ_N this boundary condition will contribute to the coercivity of the problem and the problem is well-posed.

The corresponding *discrete dual problem* then requires to find $z_h \in S_h^{\mathfrak{p}}$ such that

$$a_h(\psi_h, z_h) = J(\psi_h) \quad \forall\,\psi_h \in S_h^{\mathfrak{p}}. \tag{2.12}$$

Definition 2.3. We say that the discrete dual problem (2.12) is *adjoint consistent* with the dual problem (2.11) if the exact solution $z \in H^2(\Omega)$ of (2.11) satisfies (2.12),

$$a_h(\psi, z) = J(\psi) \quad \forall\,\psi \in H^2(\Omega, \mathscr{T}_h). \tag{2.13}$$

In the following, we deal with the adjoint consistency of the discrete dual problem (2.12). We show that in order to guarantee the adjoint consistency, the right-hand side of (2.12) has to be slightly modified.

2.3. Adjoint consistency. Following the approach from [17], we rewrite (2.12) element-wise and by integration by parts and the definition of the forms (2.4) we get that the solution of (2.12) satisfies

$$\sum_{K\in\mathcal{T}_h}\int_K R^*(z_h)\psi_h\,\mathrm{d}x+\int_{\partial K\setminus\partial\Omega} r^*(z_h)\psi_h+\varrho^*(z_h)\nabla\mathbb{A}\psi_h\cdot\boldsymbol{n}\,\mathrm{d}S + \int_{\partial K\cap\partial\Omega} r^*_{\partial\Omega}(z_h)\psi_h+\varrho^*_{\partial\Omega}(z_h)\mathbb{A}\nabla\psi_h\cdot\boldsymbol{n}\,\mathrm{d}S=0\quad\forall\,\psi_h\in S_h^{\mathfrak{p}}, \tag{2.14}$$

where the dual residuals consist of the volume part $R^*(z_h)=j_\Omega+\Delta z_h+\boldsymbol{b}\cdot\nabla z_h-cz_h$, parts over the interior edges

$$\begin{aligned} r^*(z_h)&=-\tfrac{1}{2}[\![\mathbb{A}\nabla z_h]\!]+(1-\theta)\langle\mathbb{A}\nabla z_h\rangle\cdot\boldsymbol{n}-(\sigma+\boldsymbol{b}\cdot\boldsymbol{n}_K)[\![z_h]\!],\\ \varrho^*(z_h)&=\tfrac{1}{2}[\![z_h]\!], \end{aligned} \tag{2.15}$$

and finally of the boundary terms

$$\begin{aligned} r^*_{\partial\Omega}(z_h)&=-(1-\theta)\mathbb{A}\nabla z_h\cdot\boldsymbol{n}-\sigma z_h \quad \text{on } \partial K^-\cap\Gamma_D,\\ r^*_{\partial\Omega}(z_h)&=-(1-\theta)\mathbb{A}\nabla z_h\cdot\boldsymbol{n}-\sigma z_h-\boldsymbol{b}\cdot\boldsymbol{n}z_h \quad \text{on } \partial K^+\cap\Gamma_D,\\ r^*_{\partial\Omega}(z_h)&=j_{\Gamma_N}-\mathbb{A}\nabla z_h\cdot\boldsymbol{n}-\boldsymbol{b}\cdot\boldsymbol{n}z_h \quad \text{on } \partial K\cap\Gamma_N,\\ r^*_{\partial\Omega}(z_h)&=j_{\Gamma_N}-\boldsymbol{b}\cdot\boldsymbol{n}z_h \quad \text{on } \partial K\cap\Gamma_+,\\ r^*_{\partial\Omega}(z_h)&=0 \quad \text{on } \partial K\cap\Gamma_-,\\ \varrho^*_{\partial\Omega}(z_h)&=(j_{\Gamma_D}+z_h) \quad \text{on } \Gamma_D,\\ \varrho^*_{\partial\Omega}(z_h)&=0 \quad \text{elsewhere on } \partial\Omega. \end{aligned} \tag{2.16}$$

Concerning the symmetric variant of DG we see that if $z\in H^2(\Omega)$ is the solution of the problem (2.11), it nullifies the volume residual R^* and also all residuals on interior edges and boundary edges except Γ_D. On Γ_D we have $z=-j_{\Gamma_D}$ from $\varrho^*_{\partial\Omega}$, but also $\sigma z+\boldsymbol{b}\cdot\boldsymbol{n}z=0$ on $\partial K^+\cap\Gamma_D$ and $\sigma z=0$ on $\partial K^-\cap\Gamma_D$, which are in conflict unless $j_{\Gamma_D}=0$.

This problem can be overcome by a small modification of the target functional according to the method from [17]. We define

$$r_J(v):=\begin{cases}-\sigma(v-u_D)j_{\Gamma_D} & \text{on } \partial K^-\cap\Gamma_D\\ -(\sigma+\boldsymbol{b}\cdot\boldsymbol{n})(v-u_D)j_{\Gamma_D} & \text{on } \partial K^+\cap\Gamma_D\end{cases} \tag{2.17}$$

and then

$$\tilde{J}(v):=J(v)+\int_{\Gamma_D} r_J(v)\,\mathrm{d}S. \tag{2.18}$$

The modification is designed so that $\tilde{J}(u) = J(u)$ for u being the exact solution of the problem (2.1). Further, since $\tilde{J}(v)$ is affine, we have $\tilde{J}(u) - \tilde{J}(u_h) = \tilde{J}'_u(u - u_h)$, where

$$\tilde{J}'_u(v) = J(v) - \sum_{K\in\mathcal{T}_h} \left(\int_{\Gamma_D\cap\partial K^-} v\sigma j_{\Gamma_D}\,\mathrm{d}S - \int_{\Gamma_D\cap\partial K^+} v(\sigma + \boldsymbol{b}\cdot\boldsymbol{n}) j_{\Gamma_D}\,\mathrm{d}S \right) \tag{2.19}$$

is the Gateaux derivative of $\tilde{J}$ in direction v. In order to guarantee the adjoint consistency of the dual problem, we can replace the dual problem (2.12) by

$$a_h(\psi_h, z_h) = \tilde{J}'_u(\psi_h) \quad \forall\, \psi_h \in S_h^{\mathfrak{p}}. \tag{2.20}$$

All the derivations presented in Subsection 2.3 can be summarized into the following result.

Lemma 2.2. *The SIPG method is the adjoint consistent discretization* (2.20) *of the problem* (2.1) *with target functionals defined according to* (2.18). *Moreover, it provides the Galerkin orthogonality also for the dual solutions z and z_h:*

$$a_h(\psi_h, z - z_h) = 0 \quad \forall\, \psi_h \in S_h^{\mathfrak{p}}. \tag{2.21}$$

On the other hand, for nonsymmetric variants ($\theta \in \{-1, 0\}$) the dual discretization is surely not adjoint consistent with (2.11) due to $\langle \mathbb{A}\nabla z\rangle \neq 0$ in (2.15). Therefore, we limit our further steps only to the SIPG variant. In the following, we will use the notation J instead of $\tilde{J}$, for simplicity.

2.4. Goal-oriented error estimates. Using the adjoint consistency (2.13), the consistency (2.8), the Galerkin orthogonality of the error (2.9), we get the *primal error identity* for the error of the quantity of interest

$$\begin{aligned} J(u - u_h) &= a_h(u - u_h, z) = l_h(z) - a_h(u_h, z) =: r_h(u_h)(z) \\ &= r_h(u_h)(z - \varphi_h) \quad \forall\, \varphi_h \in S_h^{\mathfrak{p}}, \end{aligned} \tag{2.22}$$

where $r_h(u_h)(\cdot)$ denotes the residual of the problem (2.7). Let us note that the Galerkin orthogonality was used only in the last step, i.e., the identity $J(u - u_h) = r_h(u_h)(z)$ is valid also for u_h violating the Galerkin orthogonality, which is the case of the approximate solution suffering from algebraic errors.

Similarly, exploiting (2.21), we get the *dual error identity*

$$\begin{aligned} J(u - u_h) &= a_h(u - u_h, z - z_h) = a_h(u - \psi_h, z - z_h) \\ &= J(u - \psi_h) - a_h(u - \psi_h, z_h) =: r_h^*(z_h)(u - \psi_h) \quad \forall\, \psi_h \in S_h^{\mathfrak{p}}, \end{aligned} \tag{2.23}$$

where $r_h^*(z_h)(\cdot)$ denotes the residual of the dual problem (2.12).

Hence, the residuals $r_h(u_h)(\cdot)$ and $r_h^*(z_h)(\cdot)$ are equal in the following way:

$$r_h(u_h)(z-\varphi_h) = r_h^*(z_h)(u-\psi_h) \quad \forall\, \varphi_h, \psi_h \in S_h^{\mathfrak{p}}. \tag{2.24}$$

3. Reconstruction of the discrete solution

Except for a very few examples, neither u nor z are a priori known. Therefore, they must be replaced by some computable quantities in (2.22) and (2.23). In particular, we define

$$\eta_{\mathrm{S}} := r_h(u_h)(z_h^+ - \varphi_h), \quad \eta_{\mathrm{S}}^* := r_h^*(z_h)(u_h^+ - \varphi_h). \tag{3.1}$$

Obviously the functions z_h^+ and u_h^+ must be from a richer space than $S_h^{\mathfrak{p}}$ otherwise the residuals would degenerate, since $r_h(u_h)(\varphi_h) = r_h^*(z_h)(\varphi_h) = 0$ for all $\varphi_h \in V_h$.

We get the following equality for the error (primal formulation):

$$\begin{aligned} J(u-u_h) = r_h(u_h)(z-\varphi_h) &= r_h(u_h)(z_h^+ - \varphi_h) + r_h(u_h)(z - z_h^+) \\ &:= \eta_{\mathrm{S}} + \varepsilon_S \quad \forall\, \varphi_h \in S_h^{\mathfrak{p}}. \end{aligned} \tag{3.2}$$

The first term on the right-hand side is computable. The second term is usually neglected, e.g. [4], with the idea that it should be negligible in comparison with η_{S}.

Naturally, the size of ε_S depends on the quality of the approximation z_h^+. Exploiting the boundedness of the bilinear form $a_h(u,v) \leqslant \|u\|_{\mathrm{DG}}\|v\|_{\mathrm{DG}}$ in the DG-norm $\|\cdot\|_{\mathrm{DG}}$, see e.g. [9], Section 4.6 or [26], we can write

$$\varepsilon_S = a_h(u-u_h, z-z_h^+) \leqslant \|u-u_h\|_{\mathrm{DG}}\|z-z_h^+\|_{\mathrm{DG}}. \tag{3.3}$$

Having an a priori estimate $\|z-z_h^+\|_{\mathrm{DG}} \leqslant Ch^{p+k}$, $k>0$, while $\|z-z_h\|_{\mathrm{DG}} \leqslant Ch^p$ only, leads to the assumption that ε_S should be significantly smaller than η_{S} on fine meshes. Conversely, in [22] it was shown that estimates using η_{S} only, significantly underestimate the error on coarse meshes, which may lead to stopping the adaptive procedure even when the true error is still large.

3.1. Error indicators. Employing these estimates for mesh adaptation requires to localize (3.1) into positive error indicators describing local error contributions.

In conforming FEM this is usually done by plugging some partition of unity into (3.1) (see e.g. [24]). In DG discretization we simply define element-wise contributions of (3.1)

$$\eta_{\mathrm{S,K}} = |r_h(u_h)((z_h^+ - \varphi_h)\chi_K)|, \quad \eta_{\mathrm{S,K}}^* = |r_h^*(z_h)((u_h^+ - \varphi_h)\chi_K)|, \quad K \in \mathcal{T}_h, \tag{3.4}$$

which corresponds to a partition of unity formed of the characteristic functions of mesh elements, i.e. $1 = \sum_{K \in \mathcal{T}_h} \chi_K$, plugged into (3.1).

Either of those can be used as a local error indicator for mesh refinement. Although the primal and dual residuals are theoretically equivalent, cf. (2.24), localizations (3.4) can differ notably and may lead to differently refined meshes.

The functional J generally does not have the additive property such as norms and can attain both positive and negative values on different elements. Therefore, we cannot expect that the sum of the local error indicators would sharply approximate the total error $J(u) - J(u_h)$.

The standard approach for approximating (2.22) is to compute the dual problem on a finer mesh or with higher polynomial degree, see [18]. E.g. in [25] the authors compute the so-called reference solutions $u_h^+, z_h^+ \in S_{h/2}^{p+1}$ on a globally refined mesh with increased polynomial degree. Although this method achieves very precise results, it is too time consuming, since it requires a solution of a globally enlarged system.

More efficiently (but also more heuristically) u_h^+ and z_h^+ may be computed by a local reconstruction of the discrete solutions u_h and z_h, respectively. For conforming finite element methods mostly reconstructions based on some patch-wise higher-order interpolation are used, e.g. in [21], [24], [23]. None of those methods are applicable to DG due to the discontinuity of functions in $S_h^{\mathfrak{p}}$. We are not aware of any paper, where a local reconstruction of the DG solution would be used to goal-oriented estimates, even though, for instance, the reconstruction based on orthogonal polynomials from [20] may be applicable on quadrilateral meshes.

We present two methods applicable to DG of an arbitrary degree (even *hp*-variant). None of these methods requires any patch-wise structure of the mesh. This is very favorable, since we aim for the combination of the DWR estimates with the anisotropic mesh generator [7]. We present the ideas for reconstruction of the discrete solution u_h, computation of z_h^+ being done alike using the function z_h.

3.2. Weighted least-square method. First, we employ the method developed in [12]. For the purpose of the presented reconstruction we define the space $S_h^{\mathfrak{p}+1} := \{v \in L^2(\Omega);\ v\big|_K \in P^{p_k+1}(K)\ \forall K \in \mathcal{T}_h.\}$ Obviously $S_h^{\mathfrak{p}} \subset S_h^{\mathfrak{p}+1} \subset H^2(\Omega, \mathcal{T}_h)$.

Let $u_h \in S_h^{\mathfrak{p}}$ be the approximate solution of (2.7). For the reconstruction $u_h^+ \in S_h^{\mathfrak{p}+1}$ on an element $K \in \mathcal{T}_h$ we use a weighted least-square approximation from the elements sharing at least a vertex with K, see Figure 2, left. We denote this patch of elements $\mathscr{D}_K = \{K' \in \mathcal{T}_h;\ K' \cap K \neq \emptyset\}$.

We compute the function $u_K^+ \in P^{p_K+1}(\mathscr{D}_K)$ by

$$u_K^+ = \operatorname*{arg\,min}_{U_h \in P^{p_K+1}(\mathscr{D}_K)} \sum_{K' \in \mathscr{D}_K} \omega_{K'} \|U_h - u_h\|^2_{H^1(K')}. \tag{3.5}$$

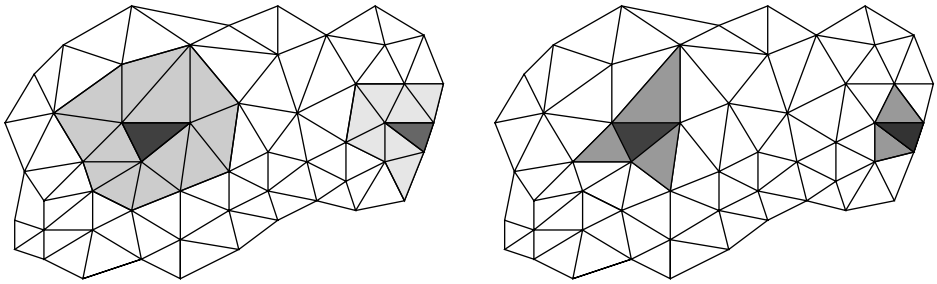

Figure 2. Examples of patches $\mathscr{D}_K$ corresponding to interior and boundary elements, large (left) and small (right) patches.

Then we assemble the higher-order reconstruction u_h^+ as an element-wise composition of $u_K^+\big|_K$, i.e. $u_h^+ = \sum_{K\in\mathcal{T}_h} u_K^+\big|_K$. In the following we will refer to this method as the LS reconstruction.

When choosing the values of the weights $\omega_{K'}$, we distinguish between elements sharing a face and elements having only a common vertex. We set $\omega_{K'} = 1$ if $K' = K$ or if K, K' share a face and $\omega_{K'} = \varepsilon$ if K, K' share only a vertex. The parameter ε helps to stabilize the reconstruction when local polynomial degrees are too varying on $\mathscr{D}_K$. Hence, we choose

$$\varepsilon := \overline{\varepsilon}\max(0, \Delta p_K - 1), \text{ where } \Delta p_k = \max_{K'\in\mathscr{D}_K} p_{K'} - \min_{K'\in\mathscr{D}_K} p_{K'}, \tag{3.6}$$

where $\overline{\varepsilon} := 0.02$ was empirically chosen. Consequently, the small patches, see Figure 2 right, are used when $\Delta p_k \leqslant 1$.

This method is actually independent of the solved problem. This can be viewed as a disadvantage, since an approximation tailored specifically for the solved problem may work more accurately, but on the other hand such specialized technique may not be available for complex problems.

As shown in [10], this reconstruction can be advantageously used also to determine the anisotropic *hp*-adaptation of the mesh. Although we cannot prove theoretically that $\|u - u_h\| \approx \|u_h^+ - u_h\|$, it was numerically verified on several examples in [12].

3.3. Solving local problems. Another common method for computing a reconstruction u_h^+ in FEM computations is based on the solution of local problems defined on patches of elements, see e.g. [3], [5].

For conforming FEM applied to the Poisson problem ($\mathcal{L} := -\Delta$) the authors of [3] suggest to solve the auxiliary problems

$$\mathcal{L}u_i^+ = f \quad \text{in } \Omega_i := \operatorname{supp}\psi_i, \quad u_i^+ = u_h \text{ on } \partial\Omega_i, \tag{3.7}$$

where $\{\psi_i\}_{i=1}^M$ is a partition of unity satisfying $\sum_{i=1}^{M}\psi(x) = 1$ for all $x \in \Omega$ and each $\psi_i \geqslant 0$.

For solving (3.7) we propose to employ again the DG method, which includes the Dirichlet boundary condition only by the penalty terms. Since no inter-element continuity is required in DG, we can define these problems even element-wise setting simply $\psi_i := \chi_K$, $K \in \mathcal{T}_h$, where χ_K is the characteristic function of the element K. Namely, for each $K \in \mathscr{T}_h$ we define the function $u_K^+ \colon \Omega \to \mathbb{R}$ such that

$$
\begin{aligned}
&\text{(i)} \quad u_K^+|_{K'} := u_h|_{K'} \quad \forall\, K' \neq K,\\
&\text{(ii)} \quad u_K^+|_K \in P^{p_K+1}(K),\\
&\text{(iii)} \quad a_h(u_K^+, \varphi_h) = l_h(\varphi_h) \quad \forall\, \varphi_h \in P^{p_K+1}(K),
\end{aligned}
\tag{3.8}
$$

where a_h is the form given by (2.6). Since evidently $u_K^+ \in S_h^{\mathfrak{p}+1}$, we finally define $u_h^+ \in S_h^{\mathfrak{p}+1}$ by $u_h^+|_K := u_K^+$ for all $K \in \mathscr{T}_h$. In the rest of the paper we will refer to this kind of reconstruction as the LOC reconstruction.

In the following we show that it is not necessary to assemble and to solve problem (3.8) for each K explicitly, when we use the residual based approach from [8]. We denote by $N_K = \frac{1}{2}(p_K+1)(p_K+2)$ the number of degrees of freedom attached to the element $K \in \mathscr{T}_h$, and by $\boldsymbol{\varphi}_K = \{\varphi_{h,K}^i\}_{i=1}^{N_K}$ the basis of the space $P^{p_K}(K)$. The basis of $S_h^{\mathfrak{p}}$, denoted by $\boldsymbol{\varphi} = \{\varphi_h^i\}_{i=1}^{N_h^{\mathfrak{p}}}$, $N_h^{\mathfrak{p}} = \dim S_h^{\mathfrak{p}}$, can be assembled by the functions from $\boldsymbol{\varphi}_K$ for all $K \in \mathcal{T}_h$ extended by zero outside K. Due to the discontinuity of the functions in $S_h^{\mathfrak{p}}$ across the element edges, we can write u_h in the element-wise components $\boldsymbol{u}_K \in \mathbb{R}^{N_K}$ corresponding to $K \in \mathscr{T}_h$, i.e.,

$$
u_h = \sum_{i=1}^{N_h^{\mathfrak{p}}} U^i \varphi_h^i = \sum_{K \in \mathcal{T}_h} \boldsymbol{u}_K \cdot \boldsymbol{\varphi}_K.
$$

Denoting $\boldsymbol{f}_K := \{l_h(\varphi_{h,K}^i)\}_{i=1}^{N_K}$, the problem (2.7) can be rewritten in the block-matrix form (one block-row for each $K \in \mathscr{T}_h$)

$$
\mathbb{A}_{K,K}\boldsymbol{u}_K + \sum\nolimits_{K' \in N(K)} \mathbb{A}_{K,K'}\boldsymbol{u}'_K = \boldsymbol{f}_K \quad \forall\, K \in \mathscr{T}_h,
\tag{3.9}
$$

where $\mathbb{A}_{K,K}$ are diagonal blocks (corresponding to a_h) of size $N_K \times N_K$, $\mathbb{A}_{K,K'}$ are the off-diagonal blocks of size $N_K \times N_{K'}$ and $N(K)$ is the set of elements sharing an edge with $K \in \mathscr{T}_h$.

For each $K \in \mathcal{T}_h$, we can write $u_K^+ = u_h + \tilde{u}_K$, where u_h is the approximate solution given by (2.7) and $\tilde{u}_K \in P^{p_K+1}(K)$ can be viewed as a local higher order correction. Obviously, due to condition (i) in (3.8), we have $\tilde{u}_K = 0$ on all $K' \neq K$, $K' \in \mathscr{T}_h$.

Let $\varphi_{h,K} \in P^{p_K+1}(K)$. Using the linearity of a_h, condition (iii) in (3.8) and (2.22), we have

$$a_h(\tilde{u}_K, \varphi_{h,K}) = a_h(u_K^+, \varphi_{h,K}) - a_h(u_h, \varphi_{h,K}) = l_h(\varphi_{h,K}) - a_h(u_h, \varphi_{h,K}) \\ = r_h(u_h)(\varphi_{h,K}). \tag{3.10}$$

Hence, we have to solve

$$a(\tilde{u}_K, \varphi_{h,K}) = r_h(u_h)(\varphi_{h,K}) \quad \forall\, \varphi_{h,K} \in P^{p_K+1}(K) \tag{3.11}$$

for each $K \in \mathcal{T}_h$. We denote $N_K^+ = \dim P^{p_K+1}(K) = (p_K+2)(p_K+3)/2$ and choose a basis $\varphi_{h,K}^1, \ldots, \varphi_{h,K}^{N_K}, \ldots, \varphi_{h,K}^{N_K^+}$ of P^{p_K+1} as hierarchical extension of the basis $\boldsymbol{\varphi}_K$. Then (3.11) can be written in similar form to (3.9), where the off-diagonal terms are vanishing, since $\tilde{u}_K = 0$ on all $K' \neq K$, namely

$$\mathbb{A}_{K,K}^+ \tilde{\boldsymbol{u}}_K = \boldsymbol{r}, \tag{3.12}$$

where $\mathbb{A}_{K,K}^+ \in \mathbb{R}^{N_K^+ \times N_K^+}$ is the matrix $\mathbb{A}_{K,K}$ enlarged by $N_K^+ - N_K$ rows and columns, $\boldsymbol{r} \in \mathbb{R}^{N_K^+}$ is the vector with components $r_i = r_h(u_h)(\varphi_{h,K}^i)$, $i = 1, \ldots, N_K^+$ and $\tilde{\boldsymbol{u}}_K$ is the vector of basis coefficients defining the function $\tilde{u}_K$ on K. Let us note that first N_K components of $\boldsymbol{r}$ are vanishing up to the algebraic errors.

Therefore, in order to find the reconstruction (3.8) for each $K \in \mathcal{T}_h$, we have to assemble the block-diagonal block $\mathbb{A}_{K,K}^+$, evaluate the residual (2.22) for all basis functions of $P^{p_K+1} \setminus P^{p_K}$ and solve the linear algebraic system (3.12). Finally, we put $u_h^+ = u_h + \sum\limits_{K \in \mathcal{T}_h} \tilde{u}_K$.

R e m a r k 3.1. This method can be used even for nonlinear problems, but in that case the computation of the update $\tilde{u}_K$ has to be iterated several times.

R e m a r k 3.2. For the reconstruction based on the solution of local problems we have (in exact arithmetics) due to (2.7), (2.12), and (3.10) that

$$\eta_{\mathrm{S,K}} = r_h(u_h)(z_h^+\big|_K) = r_h(u_h)(\tilde{z}_K) = a_h(\tilde{u}_K, \tilde{z}_K) \\ = r_h^*(z_h)(\tilde{u}_K) = r_h^*(z_h)(u_h^+\big|_K) = \eta_{\mathrm{S,K}}^*. \tag{3.13}$$

Hence, we not only get the global equivalence corresponding to (2.24), but even the local error indicators $\eta_{\mathrm{S,K}}$ and $\eta_{\mathrm{S,K}}^*$ are equivalent for this reconstruction.

On the contrary, the LS reconstruction is not connected with the solved problem and the error estimates η_{S} and η_{S}^* may differ both locally and globally.

Remark 3.3. We may also solve the $a_h(u,v) = r_h(u_h)(v)$ reconstruction on patches of elements having one common vertex. This would be connected with the partition of unity using the piece-wise linear "hat" functions.

4. Algebraic errors

Due to algebraic errors neither the "exact" discrete solution u_h of (2.7) nor the solution z_h of (2.12) are available in practical computations. Instead, we compute their approximations $u_h^{(n)}$ and $z_h^{(n)}$ resulting from a finite number of iterations of an algebraic iterative solver. Considering the algebraically inexact discrete solution $u_h^{(n)}$ the Galerkin orthogonalities (2.9) and (2.21) do not hold anymore. Hence, we must add an additional term measuring the deviation from the Galerkin orthogonality due to algebraic errors. For the primal error identity (2.22) using the triangle inequality, we have

$$J(u-u_h^{(n)}) = r_h(u_h^{(n)})(z) = r_h(u_h^{(n)})(z-\varphi_h) + r_h(u_h^{(n)})(\varphi_h) \quad \forall\, \varphi_h \in S_h^{\mathtt{p}}. \tag{4.1}$$

Regarding the revision of dual estimate (2.23), we proceed similarly. Using the definitions of residuals r_h and r_h^* in (2.22) and (2.23), respectively, and the triangle inequality, we get

$$\begin{aligned} r_h(u_h^{(n)})(z-z_h^{(n)}) &= a_h(u-u_h^{(n)}, z-z_h^{(n)}) \\ &= a_h(u-\psi_h, z-z_h^{(n)}) + a_h(\psi_h-u_h^{(n)}, z-z_h^{(n)}) \\ &= r_h^*(z_h^{(n)})(u-\psi_h) + r_h^*(z_h^{(n)})(\psi_h-u_h^{(n)}) \quad \forall\, \psi_h \in S_h^{\mathtt{p}}. \end{aligned} \tag{4.2}$$

Then putting $\varphi_h := z_h^{(n)}$ in (4.1) and using (4.2), we obtain

$$J(u-u_h^{(n)}) = r_h^*(z_h^{(n)})(u-\psi_h) + r_h^*(z_h^{(n)})(\psi_h-u_h^{(n)}) + r_h(u_h^{(n)})(z_h^{(n)}) \quad \forall\, \psi_h \in S_h^{\mathtt{p}}. \tag{4.3}$$

The impact of algebraic errors in goal-oriented estimates was studied in [21], where the equivalence (2.24) is mentioned but only the estimates based on the primal residual are considered. Since this equivalence is not relevant for algebraically inexact solutions, we use both of these estimates and compare their accuracy in concrete computations (see Section 5).

The primal and dual part of the error identity in (2.22) can be separated, see e.g. [4]. Exploiting the boundedness of the bilinear form $a_h(\cdot,\cdot)$ in the DG-norm (2.5), we get

$$\begin{aligned} J(u-u_h) = a_h(u-u_h, z-\varphi_h) &= \sum_{K\in\mathcal{T}_h} a_h(u-u_h, z-\varphi_h)\big|_K \\ &\leqslant \sum_{K\in\mathcal{T}_h} |\!|\!| u-u_h |\!|\!|_{\mathrm{DG},K} |\!|\!| z-\varphi_h |\!|\!|_{\mathrm{DG},K} \quad \forall\, \varphi_h \in S_h^{\mathtt{p}}, \end{aligned} \tag{4.4}$$

where $\|\!|\cdot|\!\|_{\mathrm{DG},K}$ is the element-wise analogue of the norm $\|\!|\cdot|\!\|_{\mathrm{DG}}$ given by (2.5). Due to this separation, tightness of the estimates is strongly dependent on the choice of φ_h. On the contrary, in (2.22) the choice of φ_h is irrelevant but when those errors are taken into account as in (4.1), then the choice of φ_h may again influence the computation process. Therefore, we present three variants of (3.1):

$$\text{(4.5a)} \qquad \overline{\eta}_{\mathrm{S}}^{(n)} := r_h(u_h^{(n)})(z_h^+), \qquad \overline{\eta}_{\mathrm{S}}^{*,(n)} := r_h^*(z_h^{(n)})(u_h^+),$$

$$\text{(4.5b)} \qquad \widetilde{\eta}_{\mathrm{S}}^{(n)} := r_h(u_h^{(n)})(z_h^+ - z_h^{(n)}), \qquad \widetilde{\eta}_{\mathrm{S}}^{*,(n)} := r_h^*(z_h^{(n)})(u_h^+ - u_h^{(n)}),$$

$$\text{(4.5c)} \qquad \hat{\eta}_{\mathrm{S}}^{(n)} := r_h(u_h^{(n)})(z_h^+ - P_h^p z_h^+), \qquad \hat{\eta}_{\mathrm{S}}^{*,(n)} := r_h^*(z_h^{(n)})(u_h^+ - P_h^p u_h^+).$$

Here P_h^p denotes the L^2-orthogonal projection to S_h^{p}, i.e. for any $v \in L^2(\Omega)$ it satisfies $\int_\Omega P_h^p v \varphi_h \,\mathrm{d}x = \int_\Omega v\varphi_h \,\mathrm{d}x$ for all $\varphi_h \in S_h^{\mathrm{p}}$. Furthermore, we introduce the *primal* and *dual algebraic* error estimates

$$\text{(4.6a)} \qquad \overline{\eta}_{\mathrm{A}}^{(n)} = \widetilde{\eta}_{\mathrm{A}}^{(n)} := r_h(u_h^{(n)})(z_h^{(n)}), \qquad \overline{\eta}_{\mathrm{A}}^{*,(n)} = \widetilde{\eta}_{\mathrm{A}}^{*,(n)} := r_h^*(z_h^{(n)})(u_h^{(n)}),$$

$$\text{(4.6b)} \qquad \hat{\eta}_{\mathrm{A}}^{(n)} := r_h(u_h^{(n)})(P_h^p z_h^+), \qquad \hat{\eta}_{\mathrm{A}}^{*,(n)} := r_h^*(z_h^{(n)})(P_h^p u_h^+).$$

Since the exact specification is usually not necessary, we will talk generally about $\eta_{\mathrm{A}}^{(n)} \in \{\overline{\eta}_{\mathrm{A}}^{(n)}, \tilde{\eta}_{\mathrm{A}}^{(n)}, \hat{\eta}_{\mathrm{A}}^{(n)}\}$ and $\eta_{\mathrm{A}}^{*,(n)} \in \{\overline{\eta}_{\mathrm{A}}^{*,(n)}, \widetilde{\eta}_{\mathrm{A}}^{*,(n)}, \hat{\eta}_{\mathrm{A}}^{*,(n)}\}$. Let us note that if $u_h^{(n)}$ and $z_h^{(n)}$ satisfy the Galerkin orthogonality (2.9) and (2.21), respectively, then

$$\overline{\eta}_{\mathrm{S}}^{(n)} = \widetilde{\eta}_{\mathrm{S}}^{(n)} = \hat{\eta}_{\mathrm{S}}^{(n)}, \quad \overline{\eta}_{\mathrm{S}}^{*,(n)} = \widetilde{\eta}_{\mathrm{S}}^{*,(n)} = \hat{\eta}_{\mathrm{S}}^{*,(n)}, \quad \eta_{\mathrm{A}}^{(n)} = \eta_{\mathrm{A}}^{*,(n)} = 0.$$

R e m a r k 4.1. We may express the reconstruction of the dual solution with respect to an orthogonal basis of the space $S_h^{\mathrm{p}+1}$, i.e. $z_h^+ = \sum_{k=1}^{N_h^{\mathrm{p}+1}} z_k \varphi_k$, where $N_h^{\mathrm{p}+1} = \sum_{K\in\mathcal{T}_h} \binom{p_K+d}{d}$. Then for $\varphi_h = P_h^p z$ we get

$$\text{(4.7)} \qquad \begin{aligned} J(u - u_h^{(n)}) &= r_h(u_h^{(n)})((I - P_h^p)z_h^+) + r_h(u_h^{(n)})(P_h^p z_h^+) \\ &= \underbrace{\sum_{k=N_h^{\mathrm{p}}+1}^{N_h^{\mathrm{p}+1}} z_k r_h(u_h^{(n)})(\varphi_k)}_{\text{discretization error}} + \underbrace{\sum_{k=1}^{N_h^{\mathrm{p}}} z_k r_h(u_h^{(n)})(\varphi_k)}_{\text{algebraic error}}. \end{aligned}$$

Then the second term $\eta_{\mathrm{A}}^{(n)}$ measures the deviation of $u_h^{(n)}$ from u_h with respect to the target quantity while the first measures the discretization error weighted by the oscillations of the dual solution of degree $p+1$. The algebraic errors represent the oscillation of the lower degrees which have more global behavior and hence may strengthen the oscillations (changing signs) of the global discretization estimate.

The reconstruction of the dual solution z_h^+ used in $\eta_{\mathrm{S}}^{(n)}$ is affected by algebraic errors as well. In order to take these into account in practical computations, we monitor the value of $\eta_{\mathrm{A}}^{*,(n)}$ in error estimates based on the primal error identity (4.1) too.

4.1. Adaptive algorithm. We denote $e_h = u - u_h$ and using the error estimates (4.5) and error indicators (3.4) we propose the following adaptive algorithm.

Algorithm 1: Adaptive algorithm balancing discretization and algebraic errors

initialization: set $\eta = 2\mathrm{TOL}$;
while $\eta > \mathrm{TOL}$ **do**
  while $\eta_{\mathrm{A}}^{(n)} > C_A^{(1)}\eta_{\mathrm{S}}^{(n)}$ and $\eta_{\mathrm{A}}^{*,(n)} > C_A^{(1)}\eta_{\mathrm{S}}^{*,(n)}$ **do**
    perform GMRES iterations for primal problem (2.7);
    perform GMRES iterations for dual problem (2.12);
  end
  if $\eta_{\mathrm{A}}^{(n)} < C_A^{(1)}\eta_{\mathrm{S}}^{(n)}$ **then**
    perform GMRES iterations for dual problem until $\eta_{\mathrm{A}}^{*,(n)} < C_A^{(2)}\eta_{\mathrm{S}}^{(n)}$;
    use $\eta := \eta_{\mathrm{S}}^{(n)}$, $\eta_K := \eta_{\mathrm{S,K}}^{(n)}$;
  else
    perform GMRES iterations for primal problem until $\eta_{\mathrm{A}}^{(n)} < C_A^{(2)}\eta_{\mathrm{S}}^{*,(n)}$;
    use $\eta := \eta_{\mathrm{S}}^{*,(n)}$, $\eta_K := \eta_{\mathrm{S,K}}^{*,(n)}$;
  end
  according to error indicators η_K refine $\mathcal{T}_h$;
end

The refinement of the mesh $\mathcal{T}_h$ is done either by refining 20% of the elements with the largest error (HG), which leads to meshes with hanging nodes, or using the anisotropic strategy (AMA) from [7]. In the latter case the error indicators $\eta_{\mathrm{S,K}}$ are used in order to determine the size of the mesh elements and the approximations of the $p+1$ derivatives of both u_h and z_h are used to compute the optimal anisotropy (ratio and direction) of the triangles.

The purpose of the safety constants $C_A^{(1)}, C_A^{(2)} \leqslant 1$ is to suppress the impact of the algebraic errors on the discretization estimates, since otherwise the error indicators η_K would not produce a reasonable mesh refinement. From the numerical experiments, it seems that the primal error estimate $\eta_{\mathrm{S}}^{(n)}$ is more sensitive to algebraic errors in primal problem (and vice versa for $\eta_{\mathrm{S}}^{*,(n)}$), hence we set $C_A^{(1)} = 0.01$ and $C_A^{(2)} = 0.1$, but in many numerical experiments even the value $C_A^{(2)} = 1$ leads to stable results.

R e m a r k 4.2. It seems temping to select the more promising of the estimates η_{S} and η_{S}^* (as early as possible) and stop computing the other one. Unfortunately, having in mind the curves mapping the size of the residual for GMRES, cf. [14], which can be almost constant and then decrease to zero in one iteration, gives us the clue that it may not be possible.

5. Numerical experiments

5.1. Example 1. In the first experiment we examine the performance of the reconstructions for linear Poisson equation

$$\begin{aligned} -\Delta u &= f \text{ in } \Omega, \\ u &= 0 \text{ on } \partial\Omega, \end{aligned} \tag{5.1}$$

in the cross shaped domain $\Omega = (-2,2) \times (-1,1) \cup (-1,1) \times (-2,2)$. We chose $J(u) = |\Omega_J|^{-1} \int_\Omega j_\Omega(x) u(x)\,\mathrm{d}x$, where j_Ω is the characteristic function of the square $\Omega_J = [1.2, 1.4] \times [0.2, 0.4]$. The exact value of $J(u)$ is unknown hence we use the reference value 0.407617863684 which was computed in [1], Example 2.

First we compare the quality of the presented reconstructions—primal and dual estimate based on the LS reconstruction (3.5) denoted by η_S^{LS} and $\eta_S^{*,LS}$, the estimate based on the LOC reconstruction (3.8) (only primal, see (3.13)) denoted by η_S^{loc} and lastly the computation when the dual problem is solved with globally increased polynomial degree $p+1$ denoted by η_S^+.

In Table 1 the actual error measured with respect to the target quantity is compared to the discretization error estimates with effectivity indices measuring the ratio of $\eta_{\mathrm{S}}/J(e_h)$. We see that although the effectivity indices are below one, they maintain at the same level.

Moreover, Figure 3 shows the decrease of the error $J(e_h)$ and estimates η_S when adaptive refinement is used, and the final mesh for η_S^{loc} is shown in Figure 4. It seems that although the estimates based on the local reconstructions underestimate the true error, the resulting error indicators are not worse than those obtained by global higher order solution of the dual problem. On the contrary, especially for the finer meshes they perform even better, since the algebraic error can be more easily suppressed using the estimates (4.6a).

Further, we focus on the impact of the algebraic errors on the computation. The solution is computed with piecewise linear approximation on uniformly refined mesh with 4640 triangles.

Figure 5 shows the algebraically precise discrete solution z_h (left) and its approximation $z_h^{(n)}$ spoiled by algebraic errors obtained by 30 GMRES iterations. The

$p=1$					
N_h	$J(e_h)$	η_S^+	η_S^{loc}	η_S^{LS}	$\eta_S^{*,LS}$
290	1.24×10^{-2}	1.21×10^{-2}	6.39×10^{-3}	1.01×10^{-2}	9.62×10^{-3}
i_{eff}		(0.98)	(0.51)	(0.81)	(0.78)
1160	4.47×10^{-3}	4.36×10^{-3}	2.29×10^{-3}	3.54×10^{-3}	3.45×10^{-3}
i_{eff}		(0.97)	(0.51)	(0.79)	(0.77)
4640	1.64×10^{-3}	1.60×10^{-3}	8.31×10^{-4}	1.29×10^{-3}	1.28×10^{-3}
i_{eff}		(0.97)	(0.51)	(0.79)	(0.78)
18560	6.18×10^{-4}	5.97×10^{-4}	3.07×10^{-4}	4.82×10^{-4}	4.80×10^{-4}
i_{eff}		(0.97)	(0.50)	(0.78)	(0.77)
74240	2.35×10^{-4}	2.19×10^{-4}	1.17×10^{-4}	1.83×10^{-4}	1.83×10^{-4}
i_{eff}		(0.93)	(0.50)	(0.78)	(0.78)
$p=2$					
N_h	$J(e_h)$	η_S^+	η_S^{loc}	η_S^{LS}	$\eta_S^{*,LS}$
290	1.78×10^{-3}	1.27×10^{-3}	8.36×10^{-4}	4.54×10^{-4}	4.99×10^{-4}
i_{eff}		(0.71)	(0.46)	(0.25)	(0.28)
1160	7.02×10^{-4}	4.98×10^{-4}	3.27×10^{-4}	1.75×10^{-4}	1.79×10^{-4}
i_{eff}		(0.71)	(0.47)	(0.25)	(0.25)
4640	2.80×10^{-4}	1.99×10^{-4}	1.29×10^{-4}	7.03×10^{-5}	7.09×10^{-5}
i_{eff}		(0.71)	(0.46)	(0.25)	(0.25)
18560	1.15×10^{-4}	7.49×10^{-5}	5.09×10^{-5}	2.80×10^{-5}	2.82×10^{-5}
i_{eff}		(0.65)	(0.46)	(0.25)	(0.25)

Table 1. Example 1—error estimates of the target quantity for $p=1,2$ on uniformly refined meshes.

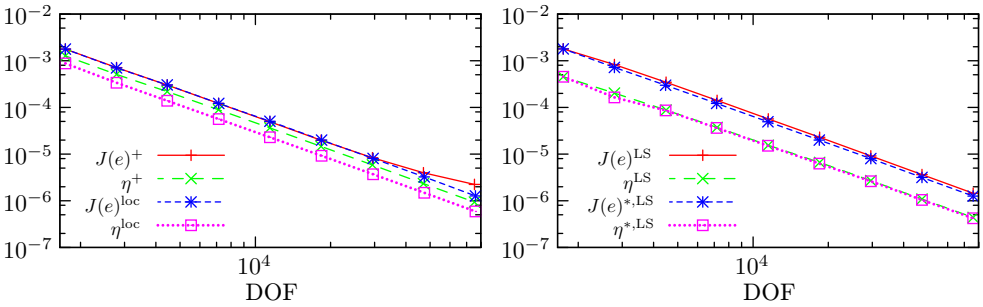

Figure 3. Example 1—decrease of $J(e_h)$ and its estimates η_{S} for $p=2$ on adaptively refined meshes.

widest contour line represents the value 10^{-4} so we see that the dual solution $z_h^{(n)}$ steadily equals zero in the major part of the domain Ω, unlike z_h.

This is caused by the local character of the quantity of interest. The right-hand side of the problem is nonzero only for basis functions having support in Ω_J and if

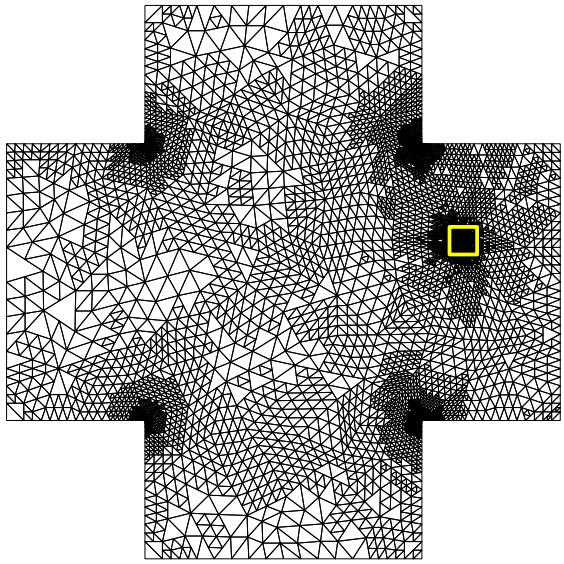

Figure 4. Example 1—Mesh with 14,417 triangles obtained by adaptive refinement based on the LOC reconstruction with Ω_J highlighted in yellow.

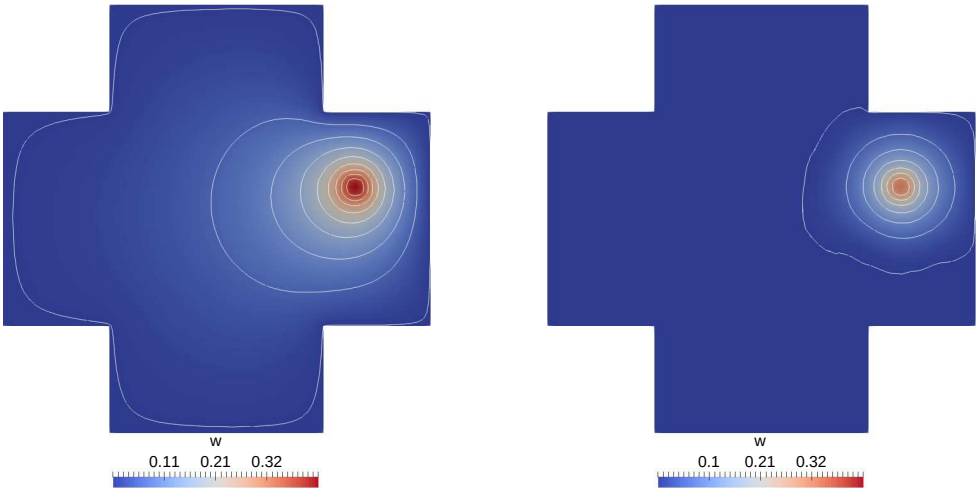

Figure 5. Example 1—algebraically precise dual solution z_h (left) and its approximation after 30 GMRES iterations (right).

we take $z_h^{(0)} = 0$ then it takes many GMRES iterations to spread the information through the whole computation domain. Since the local reconstruction of a steady zero would be again the zero function, the resulting error indicators would lead to refinement only around Ω_J and not in surroundings of the reentrant corners, where the refinement is deserving due to the irregularity of the primal solution.

In Figure 6 the differences in the mesh refinement are exhibited if 20% of the elements with largest indicators were to be refined—blue triangles would be refined due to algebraic errors while the yellow one should be refined instead. Especially, on very fine meshes this phenomenon may occur if the algebraic error was not controlled by (4.6a). A suitable preconditioning may help to overcome this phenomenon.

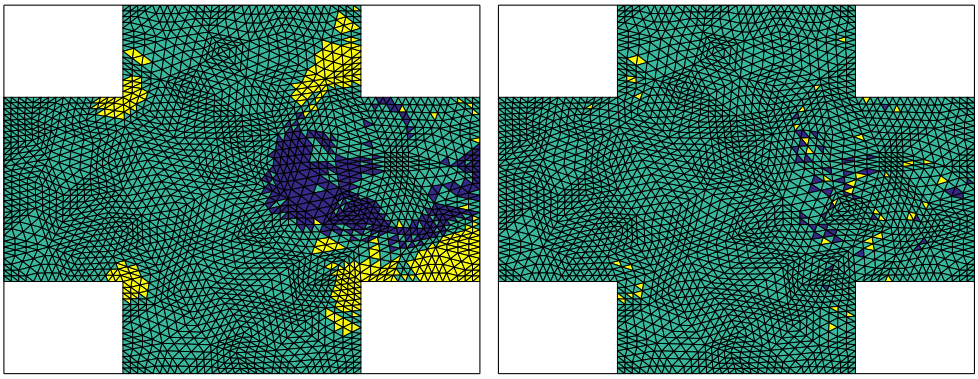

Figure 6. Example 1—differences in refinement indicators based on $\overline{\eta}_{\mathrm{S}}^{(n)}$ after 30 (left) and 180 (right) GMRES iterations using the LS reconstruction (yellow triangles should be refined instead of the blue ones).

The dependence of the error estimates on the choice of $\eta_{\mathrm{S}}^{(n)} \in \{\overline{\eta}_{\mathrm{S}}^{(n)}, \widetilde{\eta}_{\mathrm{S}}^{(n)}, \hat{\eta}_{\mathrm{S}}^{(n)}\}$, cf. (4.5), is documented in Table 2 and in Figure 7. Table 2 shows the number of differently (incorrectly) refined elements (column #) due to the algebraic errors in $\eta_{\mathrm{S}}^{(n)}$, $\eta_{\mathrm{S}}^{*,(n)}$, while Figure 7 shows the decrease of the error estimates for the least-square reconstruction. Each iteration *iter* corresponds to 50 iterations of GMRES for the primal problem and 30 iterations for the dual problem.

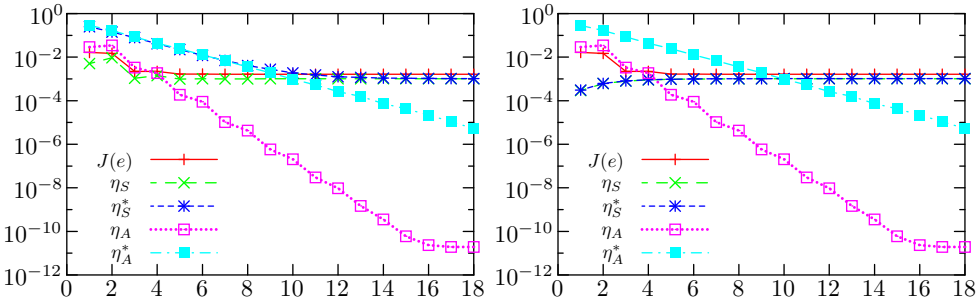

Figure 7. Example 1—error decrease during GMRES iterations for the estimates based the least-squares reconstruction, $\overline{\eta}_{\mathrm{S}}^{(n)}$ (left), $\hat{\eta}_{\mathrm{S}}^{(n)}$ (right).

The estimates $\widetilde{\eta}_{\mathrm{S}}^{(n)}$, $\hat{\eta}_{\mathrm{S}}^{(n)}$ seem to be better for the least squares reconstruction than $\overline{\eta}_{\mathrm{S}}^{(n)}$ which is very sensitive to algebraic errors. Moreover, it can be seen that

the primal estimate $\overline{\eta}_{\mathrm{S}}^{(n)}$ is more sensitive to algebraic errors in the primal problem, while $\overline{\eta}_{\mathrm{S}}^{*,(n)}$ is more sensitive to errors in the dual problem, which is in agreement with experiments performed in [11]. Estimates $\widetilde{\eta}_{\mathrm{S}}^{(n)}$ work similarly to $\hat{\eta}_{\mathrm{S}}^{(n)}$ for LS reconstruction and similarly to $\overline{\eta}_{\mathrm{S}}^{(n)}$ for LOC reconstruction. The bold zeros in Table 2 mark the step where Algorithm 15 would stop. Altogether, estimates $\hat{\eta}_{\mathrm{S}}^{(n)}$ and $\hat{\eta}_{\mathrm{S}}^{*,(n)}$ seem to be the most robust with respect to algebraic errors and can be used equivalently, cf. Table 2.

iter	$\#\overline{\eta}_S$	$\overline{\eta}_A/\overline{\eta}_S$	$\overline{\eta}^*_A/\overline{\eta}_S$	$\#\overline{\eta}^*_S$	$\overline{\eta}_A/\overline{\eta}^*_S$	$\overline{\eta}^*_A/\overline{\eta}^*_S$
2	464	3.67	1.76×10^{1}	815	2.47×10^{-1}	1.18
4	349	1.32	3.08×10^{1}	836	4.56×10^{-2}	1.06
6	45	8.80×10^{-2}	1.25×10^{1}	809	7.43×10^{-3}	1.056
8	5	4.22×10^{-3}	3.53	665	1.04×10^{-1}	8.73×10^{-1}
10	2	2.00×10^{-4}	9.47×10^{-1}	414	1.09×10^{-4}	5.13×10^{-1}
12	1	9.37×10^{-6}	2.60×10^{-1}	130	7.51×10^{-6}	2.08×10^{-1}
14	**0**	3.48×10^{-7}	7.21×10^{-2}	18	3.23×10^{-7}	6.69×10^{-2}
16	0	2.31×10^{-8}	2.16×10^{-2}	4	2.24×10^{-8}	2.10×10^{-2}
18	0	1.91×10^{-8}	5.13×10^{-3}	**0**	1.88×10^{-8}	5.04×10^{-3}
iter	$\#\hat{\eta}_S$	$\hat{\eta}_A/\hat{\eta}_S$	$\hat{\eta}^*_A/\hat{\eta}_S$	$\#\hat{\eta}^*_S$	$\hat{\eta}_A/\hat{\eta}^*_S$	$\hat{\eta}^*_A/\hat{\eta}^*_S$
2	132	5.67×10^{1}	2.72×10^{2}	129	5.53×10^{1}	2.65×10^{2}
4	38	2.06	4.80×10^{1}	35	2.03	4.73×10^{1}
6	10	9.03×10^{-2}	1.29×10^{1}	11	8.91×10^{-2}	1.27×10^{1}
8	4	4.22×10^{-3}	3.53	3	4.17×10^{-3}	3.48
10	2	2.00×10^{-4}	9.47×10^{-1}	1	1.98×10^{-4}	9.34×10^{-1}
12	1	9.37×10^{-6}	2.60×10^{-1}	0	9.24×10^{-6}	2.57×10^{-1}
14	**0**	3.48×10^{-7}	7.21×10^{-2}	**0**	3.43×10^{-7}	7.12×10^{-2}
16	0	2.31×10^{-8}	2.16×10^{-2}	0	2.28×10^{-8}	2.13×10^{-2}
18	0	1.91×10^{-8}	5.13×10^{-3}	0	1.88×10^{-8}	5.06×10^{-3}

Table 2. Example 1—number of incorrectly marked elements due to algebraic errors (LS reconstruction).

5.2. Example 2. In the second example we investigate the performance of the described method for the discretization of elliptic problem (2.1) from [16], Example 2. We set $\Omega = (0,1)^2$ and $\mathbb{A} = \varepsilon\mathbb{I}$, where

$$\varepsilon = \frac{\delta}{2}\Big(1 - \tanh\frac{(r-\frac{1}{4})(r+\frac{1}{4})}{\gamma}\Big),$$

$r = \sqrt{(x-\frac{1}{2})^2 + (y-\frac{1}{2})^2}$ and $\delta > 0$, $\gamma > 0$ are constants. Further, we suppose that $\boldsymbol{b} = (2y^2 - 4x + 1, y + 1)$, $c = -\nabla\cdot\boldsymbol{b} = 3$, and $f = 0$. We choose $\delta = 0.01$

and $\gamma = 0.05$. In this case, the diffusion coefficient ε will be approximately equal to δ in the circle with center $[\frac{1}{2}, \frac{1}{2}]$ and diameter $\frac{1}{4}$. As r increases over $\frac{1}{4}$, ε quickly decreases reaching values very close to zero ($\approx 10^{-16}$) at the boundary. Therefore, from the computational view the problem behaves like a mixed hyperbolic-elliptic problem, since convection is dominating in the region where $r > \frac{1}{4}$.

The characteristics associated with the convective part of the operator enter the domain Ω through the horizontal edge along $y = 0$ and through the vertical edges along $x = 0$ and $x = 1$. We prescribe the Dirichlet boundary condition on this "inflow" part of the boundary $\Gamma_D = \{(x, y) \in \partial\Omega\colon\ x = 0 \text{ or } x = 1 \text{ or } y = 0\}$,

$$u_D = \begin{cases} 1 & \text{if } x = 0 \text{ and } 0 < y \leqslant 1, \\ \sin^2(\pi x) & \text{if } 0 \leqslant x \leqslant 1 \text{ and } y = 0, \\ \mathrm{e}^{-50y^4} & \text{if } x = 1 \text{ and } 0 < y \leqslant 1, \end{cases} \tag{5.2}$$

which leads to discontinuities in the solution. On the rest of the boundary $\partial\Omega \setminus \Gamma_D$ we prescribe homogeneous the Neumann boundary condition.

We choose the target functional as an integral over part of the Neumann boundary

$$J(u) = \int_{0.25}^{0.625} u(x, 1)\,\mathrm{d}x \approx 0.324{,}026{,}769{,}433{,}093. \tag{5.3}$$

Since the exact solution is unknown we used the reference value $J(u)$ computed with $p = 4$ on adaptively refined mesh with more than ten thousands elements. We note that due to steep changes of the coefficients $\mathbb{A}(x)$, $\boldsymbol{b}(x)$, the evaluation of the total error (and hence also of the error estimates η_S, η_S^*) is polluted by the errors in numerical integration. The estimates of the quadrature errors are not considered in the presented approach, hence we used an overkill degree of numerical quadrature to suppress these errors.

The isocurves of the solution are pictured in the left panel of Figure 8. In Table 3 the decrease of the error of the target functional $J(e_h)$ is listed together with the effectivity indices (in brackets) for piece-wise linear DG on adaptively refined meshes. In the left panel of Figure 9 estimates η_S^{LS} and η_S^+ are compared to $J(e_h)$ when the anisotropic mesh adaptation method is employed. The decrease of the error is slightly faster in this case since some number of degrees of freedom can be reduced by the shape optimization of the triangles. In the right panel of Figure 9 estimates $\eta_S^{*,LS}$ and η_S^{loc} are compared to $J(e_h)$ for $p = 2$ with HG refinement. We can see that although the decrease of $J(e_h)$ is not monotone the error estimates η_{S} are able to capture its behavior. Note that the $\eta_S^{*,LS}$ estimate almost equals the true error on fine meshes.

η_S^+		η_S^{loc}		η_S^{LS}		$\eta_S^{*,LS}$	
N_h	$J(e_h)$	N_h	$J(e_h)$	N_h	$J(e_h)$	N_h	$J(e_h)$
128	2.02×10^{-3}	128	2.02×10^{-3}	128	2.02×10^{-3}	128	2.02×10^{-3}
	(0.96)		(0.26)		(0.55)		(0.90)
203	9.12×10^{-4}	203	1.12×10^{-3}	203	1.37×10^{-3}	203	1.48×10^{-3}
	(1.04)		(0.24)		(0.31)		(0.80)
323	2.99×10^{-4}	350	6.67×10^{-4}	323	4.40×10^{-4}	338	5.75×10^{-4}
	(1.11)		(0.56)		(0.53)		(0.91)
536	1.89×10^{-4}	566	2.45×10^{-4}	518	2.20×10^{-4}	560	2.99×10^{-4}
	(1.00)		(0.16)		(0.64)		(0.77)
899	9.77×10^{-5}	938	2.14×10^{-4}	839	1.53×10^{-4}	935	1.13×10^{-4}
	(1.04)		(0.66)		(0.50)		(0.93)
1460	5.31×10^{-5}	1541	9.49×10^{-5}	1367	7.96×10^{-5}	1541	5.23×10^{-5}
	(1.08)		(0.20)		(0.53)		(0.87)
2381	2.17×10^{-5}	2543	5.67×10^{-5}	2198	2.58×10^{-5}	2555	2.42×10^{-5}
	(0.99)		(0.30)		(0.94)		(1.12)
3899	1.42×10^{-5}	4157	3.42×10^{-5}	3569	1.65×10^{-5}	4160	8.56×10^{-6}
	(1.00)		(0.47)		(0.94)		(1.27)
6305	1.00×10^{-5}	6755	1.87×10^{-5}	5765	1.18×10^{-5}	6758	1.02×10^{-5}
	(1.00)		(0.26)		(0.89)		(0.88)
10223	4.59×10^{-6}	10961	1.03×10^{-5}	9272	5.29×10^{-6}	10958	4.52×10^{-6}
	(1.00)		(0.58)		(0.80)		(0.93)
16475	3.07×10^{-6}	17723	5.12×10^{-6}	14927	3.61×10^{-6}	17708	3.22×10^{-6}
	(1.04)		(0.39)		(0.90)		(0.97)

Table 3. Example 2—decrease of $J(e_h)$ and the corresponding effectivity indices for HG refinement and $p = 1$.

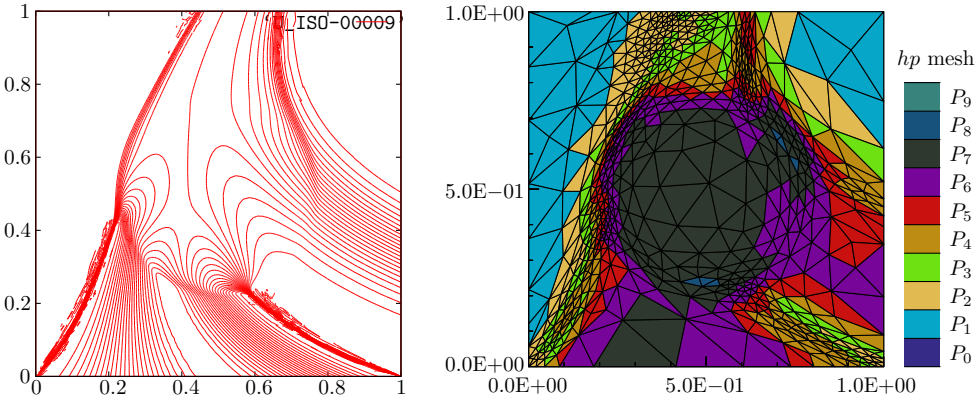

Figure 8. Example 2—primal solution (left) on final mesh (right) after *hp* anisotropic refinement.

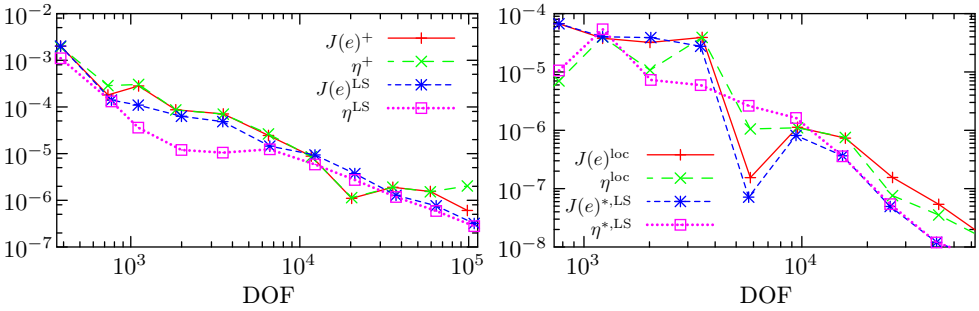

Figure 9. Example 2—error decrease for $p = 1$ anisotropic refinements (left) and $p = 2$ HG refinement (right).

Finally, in Figure 10 we present the decrease of $J(e_h)$ on adaptively refined meshes using the error indicators η_S^{LS}. We compare the results for $p = 1, 3$ using HG refinement, anisotropic refinement and the results of hp-anisotropic refinement. The final mesh of this method is shown in Figure 8 on the right. We see that this method is very efficient reaching $J(e_h) < 10^{-10}$ with only 22,861 degrees of freedom.

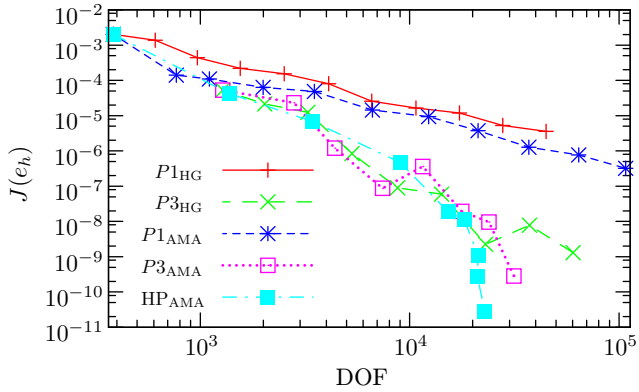

Figure 10. Example 2—decrease of the error of the target quantity on adaptively refined meshes using η_S^{LS}.

6. Conclusion

In this paper, we have presented a complex strategy for estimating the computational errors with respect to some given quantity of interest. We described an adjoint consistent discontinuous Galerkin discretization of the linear convection-diffusion-reaction problem and introduced goal-oriented estimates for both the discretization and algebraic errors.

Two kinds of local reconstructions of the DG solution were proposed. Our method suffers from the common deficiency of DWR approach—due to the approximation of the dual solution z we cannot provide guaranteed upper bound for the error of the quantity of interest. On the other hand, it provides results comparable to the approaches based on globally higher order solutions, but due to the local characteristics of the reconstructions it can be computed much faster and straightforwardly in parallel. The main advantage of the presented strategy is its application to the error indicators driving adaptive mesh refinement, where it provides very reliable results.

Further, we described the influence of the algebraic errors on the estimates based on the primal and dual residual, respectively, and we introduced a stopping criterion keeping the algebraic errors controlled by the discretization estimate. In this way the algebraic system may be solved efficiently with satisfactory accuracy with respect to the quantity of interest. On coarse meshes even quite inaccurate solution of the algebraic problem is sufficient while on fine meshes the algebraic error estimate gives us a valuable information about the level of precision which has to be reached.

References

[1] *M. Ainsworth, R. Rankin*: Guaranteed computable bounds on quantities of interest in finite element computations. Int. J. Numer. Methods Eng. *89* (2012), 1605–1634. zbl MR doi

[2] *M. Arioli, J. Liesen, A. Międlar, Z. Strakoš*: Interplay between discretization and algebraic computation in adaptive numerical solution of elliptic PDE problems. GAMM-Mitt. *36* (2013), 102–129. zbl MR doi

[3] *I. Babuška, W. C. Rheinboldt*: Error estimates for adaptive finite element computations. SIAM J. Numer. Anal. *15* (1978), 736–754. zbl MR doi

[4] *W. Bangerth, R. Rannacher*: Adaptive Finite Element Methods for Differential Equations. Lectures in Mathematics, ETH Zürich, Birkhäuser, Basel, 2003. zbl MR doi

[5] *R. E. Bank, A. Weiser*: Some a posteriori error estimators for elliptic partial differential equations. Math. Comput. *44* (1985), 283–301. zbl MR doi

[6] *R. Becker, R. Rannacher*: An optimal control approach to a posteriori error estimation in finite element methods. Acta Numerica *10* (2001), 1–102. zbl MR doi

[7] *V. Dolejší*: ANGENER—software package. Charles University Prague, Faculty of Mathematics and Physics, `www.karlin.mff.cuni.cz/~dolejsi/angen/angen.htm` (2000).

[8] *V. Dolejší*: *hp*-DGFEM for nonlinear convection-diffusion problems. Math. Comput. Simul. *87* (2013), 87–118. MR doi

[9] *V. Dolejší, M. Feistauer*: Discontinuous Galerkin Method. Analysis and Applications to Compressible Flow. Springer Series in Computational Mathematics 48, Springer, Cham, 2015. zbl MR doi

[10] *V. Dolejší, G. May, F. Roskovec, P. Šolín*: Anisotropic *hp*-mesh optimization technique based on the continuous mesh and error models. Comput. Math. Appl. *74* (2017), 45–63. zbl MR doi

[11] *V. Dolejší, F. Roskovec*: Goal oriented a posteriori error estimates for the discontinuos Galerkin method. Programs and Algorithms of Numerical Mathematics 18, Proceedings of Seminar, Janov nad Nisou 2016 (J. Chleboun et al., eds.). Institute of Mathematics CAS, Praha, 2017, pp. 15–23. doi

[12] *V. Dolejší, P. Šolín*: *hp*-discontinuous Galerkin method based on local higher order reconstruction. Appl. Math. Comput. *279* (2016), 219–235. MR doi

[13] *M. Giles, E. Süli*: Adjoint methods for PDEs: a posteriori error analysis and postprocessing by duality. Acta Numerica *11* (2002), 145–236. zbl MR doi
[14] *A. Greenbaum, V. Pták, Z. Strakoš*: Any nonincreasing convergence curve is possible for GMRES. SIAM J. Matrix Anal. Appl. *17* (1996), 465–469. zbl MR doi
[15] *K. Harriman, D. Gavaghan, E. Süli*: The importance of adjoint consistency in the approximation of linear functionals using the discontinuous Galerkin finite element method. Technical Report, Oxford University Computing Laboratory, Oxford (2004).
[16] *K. Harriman, P. Houston, B. Senior, E. Süli*: *hp*-version discontinuous Galerkin methods with interior penalty for partial differential equations with nonnegative characteristic form. Recent Advances in Scientific Computing and Partial Differential Equations, Hong Kong 2002 (S. Y. Cheng et al., eds.). Contemp. Math. 330, American Mathematical Society, Providence, 2003, pp. 89–119. zbl MR doi
[17] *R. Hartmann*: Adjoint consistency analysis of discontinuous Galerkin discretizations. SIAM J. Numer. Anal. *45* (2007), 2671–2696. zbl MR doi
[18] *R. Hartmann, P. Houston*: Symmetric interior penalty DG methods for the compressible Navier-Stokes equations. II. Goal-oriented a posteriori error estimation. Int. J. Numer. Anal. Model. *3* (2006), 141–162. zbl MR
[19] *P. Houston, C. Schwab, E. Süli*: Discontinuous *hp*-finite element methods for advection-diffusion-reaction problems. SIAM J. Numer. Anal. *39* (2002), 2133–2163. zbl MR doi
[20] *H. T. Huynh*: A reconstruction approach to high-order schemes including discontinuous Galerkin for diffusion. 18th AIAA Computational Fluid Dynamics Conference, Miami, Florida, 2007. doi
[21] *D. Meidner, R. Rannacher, J. Vihharev*: Goal-oriented error control of the iterative solution of finite element equations. J. Numer. Anal. *17* (2009), 143–172. zbl MR doi
[22] *R. H. Nochetto, A. Veeser, M. Verani*: A safeguarded dual weighted residual method. IMA J. Numer. Anal. *29* (2009), 126–140. zbl MR doi
[23] *R. Rannacher, J. Vihharev*: Adaptive finite element analysis of nonlinear problems: balancing of discretization and iteration errors. J. Numer. Math. *21* (2013), 23–62. zbl MR doi
[24] *T. Richter, T. Wick*: Variational localizations of the dual weighted residual estimator. J. Comput. Appl. Math. *279* (2015), 192–208. zbl MR doi
[25] *P. Šolín, L. Demkowicz*: Goal-oriented *hp*-adaptivity for elliptic problems. Comput. Methods Appl. Mech. Eng. *193* (2004), 449–468. zbl MR doi
[26] *E. Süli, P. Houston, C. Schwab*: *hp*-DGFEM for partial differential equations with nonnegative characteristic form. Discontinuous Galerkin Methods. Theory, Computation and Applications, Newport 1999 (B. Cockburn et al., eds.). Lect. Notes Comput. Sci. Eng. 11, Springer, Berlin, 2000, pp. 221–230. MR zbl doi

Authors' address: *Vít Dolejší*, *Filip Roskovec*, Department of Numerical Mathematics, Faculty of Mathematics and Physics, Charles University in Prague, Sokolovská 83, 186 75 Praha 8, Czech Republic, e-mail: `dolejsi@karlin.mff.cuni.cz`, `roskovec@gmail.com`.